Investigation into the Effect of Switching Frequency on the Performance of Current Controlled Inverter Employing Space Vector Modulation Technique

By

*F. M. EL-Khouly, *Y. K. EL-Behiry, M. E. EL-Shebiny and A. S. Abdel-Ghaffar*

Department of Electrical Eng., Faculty of Eng., Menoufia University, Sebin El-Kom, Egypt

**Electrical engineer at Al-Ezz steel rebars company.*

Abstract

In this paper the effect of switching frequency on the performance of the space vector modulation (SVM) current controlled three-phase PWM inverter loaded by interior permanent magnet synchronous motor (IPMSM), is investigated. The effects of the switching frequency on the stator space reference voltage vector $V_s(t)$ and then on the inverter operation modes are investigated. The idea of event driven indicative flag that on-line indicates the inverter mode of operation is presented. Computer simulation to compare the SVM performance at different switching frequencies is developed. Effects of changing the inverter dc link voltage, reference speed and mechanical load torque on the inverter modes of operation have been presented.

1- Introduction

Recent developments in high switching frequencies power devices have enabled us to develop ultrasonic carrier PWM control techniques. These high carrier frequencies have enabled us to improve the overall performance, especially for applications that require both quick response and accurate control. Mainly, current controller forces the load current to follow the command current in the same power apparatus [1]. These devices may be AC motors or uninterruptible power supplies (UPS's). Current controller techniques have become an intensive subject of research due to the offered advantages for improving the dynamic performance of high-performance AC drives, applying vector control [2. 4].

In conventional techniques of PWM such as regular sampling and subharmonics techniques the desired PWM switching points are determined according to the intersection points between the modulating wave and a triangular carrier wave at a certain switching frequency. The direct meaning of such arrangements is that the pulse position within the switching period is not controllable [2,3]. The null time is the period at which the upper three switches of inverter or the lower three switches are active and as consequence the inverter output voltage is zero. These null times are not controllable in conventional techniques It has been proved that the null times or non-conducting times ratio at pulse beginning and pulse end have a significant effect on the current harmonics [9].

Manuscript received from Eng. Y.K. EL-Behiry

Accepted on : 13 I3 I 2001

Engineering Research Journal Vol 24,No 2, 2001 Minufiya University, Faculty Of Engineering , Shebien El-Kom , Egypt , ISSN 1110-1180

Another disadvantage of the conventional techniques is the computational effort required for each one of the three phases, where the switching periods during one carrier period are usually calculated independently for each phase. This adds more burdens to any microprocessor-based system. These disadvantages have led to the development of **SVM** technique.

Space vector modulation (**SVM**) current controller is becoming more popular for providing **PWM** control for high-performance inverter fed AC drives. **SVM** is gaining substantial attention as a promising field of research. Many researches have been executed to establish a relationship between regular-sampled **PWM** and space vector modulation (**SVM**) techniques and the effect of the proportion of null states (inverter zero output voltage) [3, 7, 8]. Other researches have focused on developing a theoretical criterion for the calculating the lower order harmonics of the current wave [5,7,8]. Others have paid special attention to the stator space voltage vector (V_s) and **PWM** voltage wave and on developing voltage compensation techniques for V_s when exceeding the inverter voltage limits [6,9].

This paper is focusing on the demonstration of three-phase **PWM** inverter different modes of operation according to the approach developed in [6,9]. It is also focusing on the demonstration of the effect of the switching frequency (f_s) on the inverter modes of operation and on the stator space voltage vector (V_s). Also developing statistical relationship between f_s and the inverter modes of operation has been investigated.

Interior permanent magnet synchronous motor (**IPMSM**) has many advantages, such as higher efficiency, owing to the absence of rotor copper losses, lower no load current and much less sensitive to the motor parameter variations. Thus the **IPMSM** drive plays vitally important role in the motion-control applications in the range of low to medium power. To effectively control **IPMSM**, SVM technique is applied as a current controller on the inverter.

2- Concept of voltage space vector

For a system of balanced three-phase voltage $V_{as}(t)$, $V_{bs}(t)$ and $V_{cs}(t)$ of cycle period 2π. The space voltage vector $V_s(t)$ can be expressed as

$$V_s(t) = (V_{as}(t) + aV_{bs}(t) + a^2 V_{cs}(t)) \tag{1}$$

Where: -

$a = e^{j(2\pi/3)}$

This definition gives a practical and friendly tool to handle three-phase quantities due to the reduction of notation complexity This concept is the basis of **SVM** technique [6].

3- Inverter Mathematical Model

Figure (1) represents the switching logic of the inverter. Every two **IGBTs** on one arm are represented as one switch. The six **IGBTs** of inverter circuit are represented as three switches N_a, N_b and N_c.

If one of the two switches on the same arm is one, the upper **IGBT** is conducting. While if it is zero, the lower one is conducting. The relationship between the three switches and the inverter output voltages are described according to the following equations [1].

$$V_a^{pwm} = \frac{V_{dc}}{3.0}(2N_a - N_b - N_c) \qquad (2)$$

$$V_b^{pwm} = \frac{V_{dc}}{3.0}(2N_b - N_a - N_c) \qquad (3)$$

$$V_c^{pwm} = \frac{V_{dc}}{3.0}(2N_c - N_b - N_a) \qquad (4)$$

Where: -

V_a^{pwm}, V_b^{pwm} and V_c^{pwm}: **PWM** actual output voltage of phase a, b and c respectively.

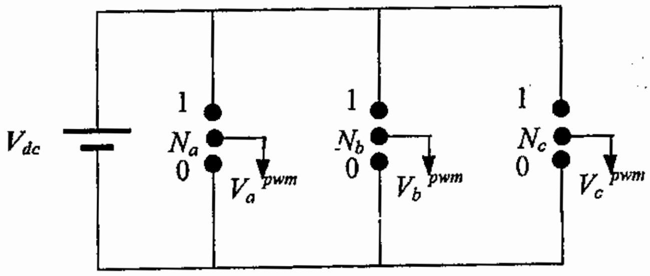

Fig. (1) Equivalent circuit of voltage source inverter.

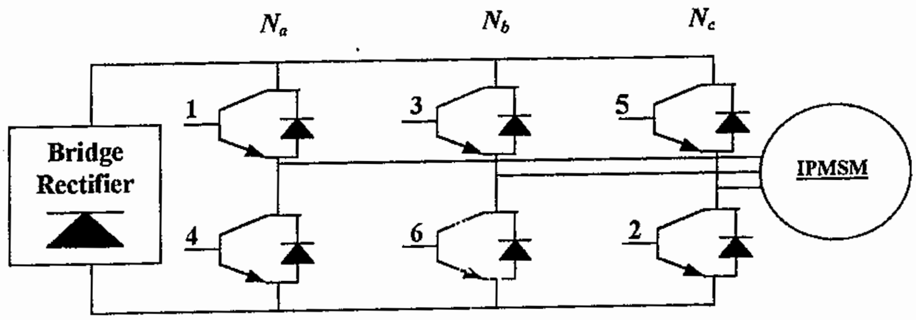

Fig. (2) Schematic diagram of inverter

	Na Nb Nc	**IGBTs**	*Vas*	*Vbs*	*Vcs*	*Vab*	*Vbc*	*Vca*
V_0	0 0 0	4 6 2	0	0	0	0	0	0
V_1	1 0 0	1 6 2	2/3	-1/3	-1/3	1	0	-1
V_2	1 1 0	1 3 2	1/3	1/3	-2/3	0	1	-1
V_3	0 1 0	4 3 2	-1/3	2/3	-1/3	-1	1	0
V_4	0 1 1	4 3 5	-2/3	1/3	1/3	-1	0	1
V_5	0 0 1	4 6 5	-1/3	-1/3	2/3	0	-1	1
V_6	1 0 1	1 6 5	1/3	-2/3	1/3	1	-1	0
V_7	1 1 1	1 3 5	0	0	0	0	0	0

Table 1 Inverter switching logic table and inverter phase and line voltage

The conduction modes of the inverter are composed of combinations of the inverter switches N_a, N_b and N_c. The detailed organization of the inverter switches is illustrated in Fig. (2). The eight switching modes of the inverter switches are demonstrated in table (1).

Recalling the concept of the voltage space vector that has demonstrated in section (2) and equations (1-4). The inverter load voltages are expressed according to equation (5).

$$V_l = \begin{cases} 0 & k = 0,7 \\ \frac{2}{3} V_{dc} e^{j(k-1)\pi/3} & k = 1,2,2,........,6 \end{cases} \qquad (5)$$

Where: -

V_l: Inverter voltage vectors

k: inverter voltage vector number that has been demonstrated in the first column in table (1).

The inverter voltage vectors are illustrated in Fig. (3).

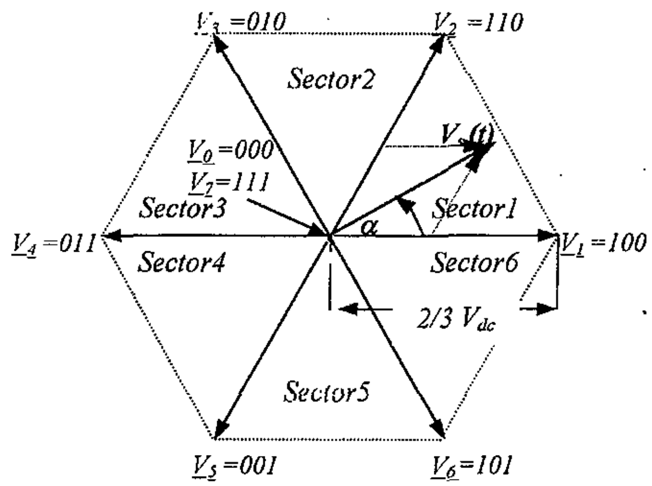

Fig. (3) Space vector V_s *(t)* and inverter voltage

4- Space vector modulation (SVM), concepts and theory

Space vector modulation is based on the concept of approximating the rotating reference voltage vector $V_s(t)$ to those that can be realized by three-phase **PWM** inverter [2,3]. This process is illustrated in Fig. (3).

As illustrated in Fig. (3) the stator space voltage vector $V_s(t)$ is superimposed on the stationary locus of the six output voltages of the inverter $(V_1, V_2, V_3 \ldots V_6)$, which is spatially oriented by $\pi/3$ intervals plus two null voltages V_0 and V_7. The voltage vector $V_s(t)$ is decomposed into its equivalent components of the eight-inverter voltage vectors according to the sector where the voltage vector is located, the conducting sequence for sector 1 will be as followed: -

$$V_0 \rightarrow V_1 \rightarrow V_2 \rightarrow V_7 \rightarrow V_7 \rightarrow V_2 \rightarrow V_1 \rightarrow V_0$$

This conducting sequence is analyzed according to the switching modes that have been mentioned before in table (1). As illustrated in Fig. (3) the first step in the conducting sequence is V_0, the inverter switches which will conduct during this step is **(4 6 2)**. The second is V_1; the conducting switches are **(1 6 2)**. The third step is V_2; the conducting switches are **(1 3 2)**. The fourth Step is V_7; the conducting switches are **(1 3 5)**. This process is repeated vice versa during the second half of the switching period **(T_s)**. **Ts** is divided into two equal halves, known and a **sampling period**. Just like regular sampling scheme, every switching period contains two equal sampling times, one for the leading edge and the other is for trailing edge. But in the contrary to regular sampling scheme, the widths of the two samples are equal and the pulse is centered inside the switching period. Also in **SVM** pulse position inside the switching period is completely controllable through changing between the null times at the beginning and the end of the switching period according to the criteria required. But in regular sampling this merit is absolutely out of the scope. The detailed process of **PWM** in **SVM** for sector 1 is illustrated in Fig. (4) [2-4]. This conducting sequence can be applied for other sectors.

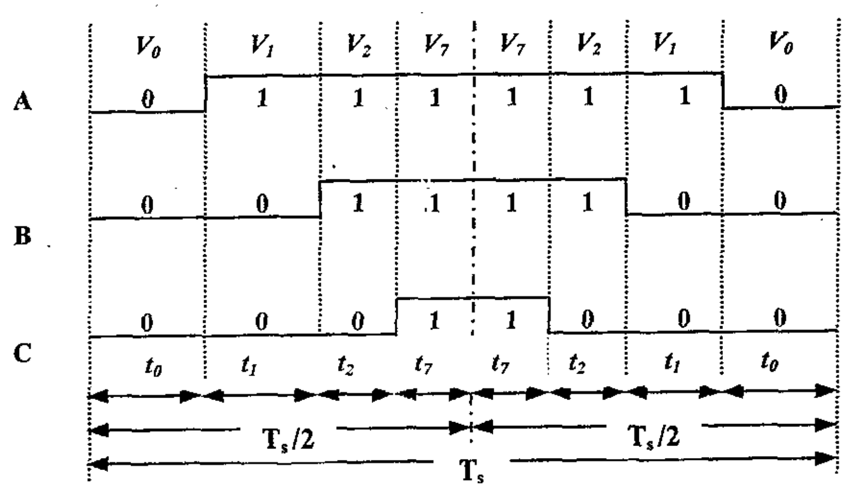

Fig. (4) Resultant three phase **PWM** waveform of one switching period

From Fig. (4), it is obvious that;

$$T_s/2 = t_0 + t_1 + t_2 + t_7 \qquad (6)$$

Where: -

$T_s/2$ is known as **sampling period.**

t_1+t_2 is known as **modulation period.**

t_0 and t_7 are known as **null periods or non-conducting periods.**

5- SVM analysis and implementation with IPMSM

The practical implementation and analysis of the SVM current controlled inverter is achieved according to the block diagram shown in Fig. (5).

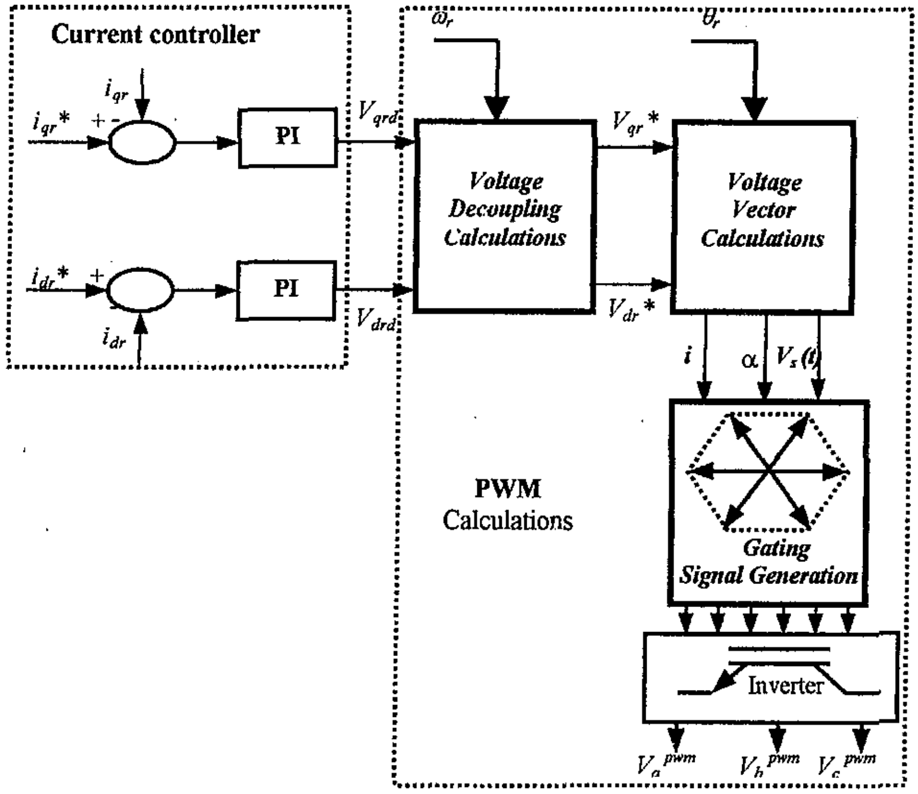

Fig. (5) Block diagram of SVM current scheme

Where: -

i_{qr}*, i_{dr}*: Synchronously rotating quadrature axis and direct axis reference currents respectively.

i_{qr}, i_{dr}: Synchronously rotating quadrature axis and direct axis actual currents respectively.

V_{qrd}, V_{drd}: Stator synchronously rotating reference voltages before decoupling circuit.

V_{qr}^*, V_{dr}^*: Stator synchronously rotating reference voltages after decoupling circuit.

α: Inclination angle.

i: Sector number.

The details of each block will be explained in the next subsections of this paper.

5.1 *PI current controllers*

Both reference and actual currents of d-axis and q-axis are compared. The error signals are manipulated through two PI controllers. The outputs are the stator voltage referred to rotor reference frame of both d-axis and q-axis.

Where: -

Kp and ***Ki:*** the **PI** current controller parameters.

$$V_{qrd} = (i_{qr}* - i_{qr}).Kp + \int Ki.(i_{qr}* - i_{qr}).dt \tag{7}$$

$$V_{drd} = (i_{dr}* - i_{dr}).Kp + \int Ki.(i_{dr}* - i_{dr}).dt \tag{8}$$

5.2 Stator Reference Voltage calculation

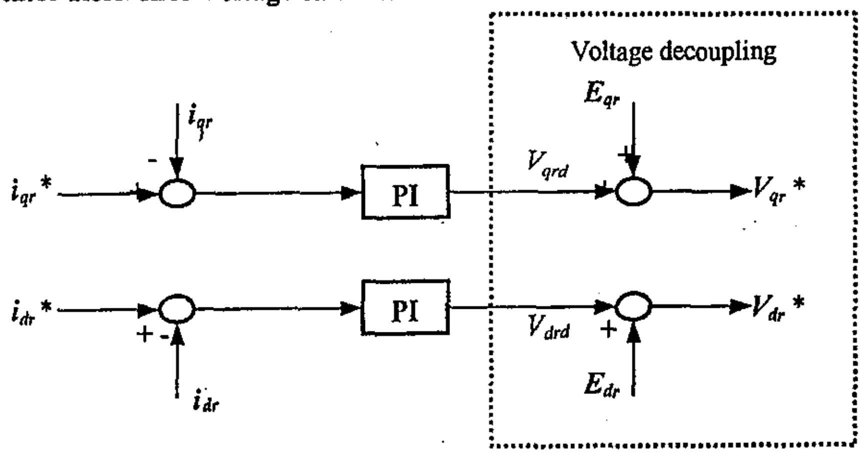

Fig. (6) **PI** current regulator with back-EMF compensation

The d-axis and q-axis currents can not be controlled independently only by V_{qrd} and V_{drd} because of the cross-coupling effects such as $\omega_r L_{qr} i_{qr}$ and $\omega_r L_{dr} i_{dr}$. These factors are dominant in electrical machines with large inductance like **IPMSM.** Therefore these factors affect both current and torque responses. The back-EMF feedforward compensation scheme is applied to reduce the effect of disturbances and to achieve d-q axis decoupling control. The details of this function are illustrated in Fig. (6).

The back- EMF of q-axis: -

$$E_{qr} = \omega_r (L_{dr}.i_{dr} + \psi_f) \tag{9}$$

The back- EMF of d-axis: -

$$E_{dr} = -\omega_r (L_{qr}.i_{qr}) \tag{10}$$

Where: -

L_{dr}, L_{qr}: direct and quadrature axis inductance, respectively.

ψ_f: constant flux linkage of permanent magnets.

ω_r: the electrical angular velocity of IPMSM.

The stator space voltage vector V_s magnitude is calculated as followed: -

$$V_s = \sqrt{V_{qr}*^2 + V_{dr}*^2} \tag{11}$$

5.3 *Gating pulses periods calculations*

These calculations are mainly based on the vector diagram demonstrated in Fig. (7). According to the concept of SVM the voltage vector is decomposed into its equivalents of eight inverter voltage vectors. This process mainly depends on inclination angle (α) and sector number (i) as explained below. Calculations of α and i are detailed in [9].

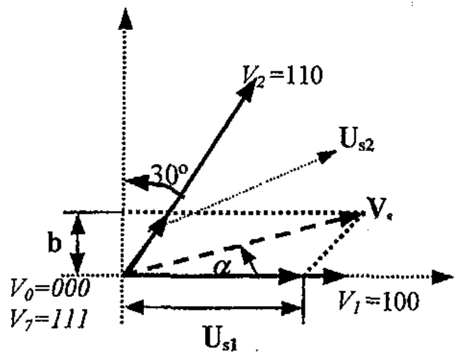

Fig. (7): Decomposition of stator space voltage vector (V_s) into inverter voltage vectors.

V_s is decomposed into its equivalent inverter voltage vectors V_1 and V_2.

$$\mathbf{U_{s2} = b/\cos(30°)} = 2b/\sqrt{3} = \mathbf{2.Vs.\sin(\alpha)/\sqrt{3}} \quad (12)$$

$$\mathbf{U_{s1} = V_s\cos(\alpha) - U_{s2}}.\cos(60°) = \mathbf{V_s\cos(\alpha) - V_s\sin(\alpha)/\sqrt{3}} \quad (13)$$

Where: -

U_{s2} and U_{s1}: Projection of voltage vector V_s into inverter vectors V_2 and V_1 respectively.

Periods, $\mathbf{t_1}$ and $\mathbf{t_2}$ are directly proportional to U_{s1} and U_{s2}, respectively. These time intervals, $\mathbf{t_1}$ and $\mathbf{t_2}$ are calculated as followed [9];

$$t_1 = 1.5.U_{s1}.T_s/V_{dc} \quad (14)$$

$$t_2 = 1.5.U_{s2}.T_s/V_{k} \quad (15)$$

By substituting equations (12-13) into equations (14-15) we get

$$\mathbf{t_2 = \sqrt{3}.V_s.\sin(\alpha).T_s/V_{dc}} \quad (16)$$

$$t_1 = \frac{3}{2}V_s.T_s(\cos(\alpha) - \frac{1}{\sqrt{3}}.\sin(\alpha))/V_{dc} \quad (17)$$

From equation (6) and considering $t_0=t_7$; then:

$$t_0 = (Ts/2 - t_1 - t_2)/2 \quad (18)$$

6- Inverter operation modes and voltage limitations

In SVM one of the most undesired behavior when the space vector $V_s(t)$ exceeds $(1/\sqrt{3})V_{dc}$. In this case the modulation periods must be rescaled to avoid negative null voltage times [9]. This rescaling process is done through the following equations: -

$$
\begin{aligned}
t_1'' &= \frac{t_1'}{t_1'+t_2'}.(T_s/2) \\
t_2'' &= \frac{t_2'}{t_1'+t_2'}.(T_s/2) \qquad (19) \\
t_0 &= t_7 = 0.0
\end{aligned}
$$

Where: -

t_1' and t_2': The modulation times for abnormal operation mode before resacling

t_1'' and t_2'': The rescaled modulation times for abnormal operation mode.

The inverter operation modes are illustrated in Fig. (8). Detailed description for every mode is demonstrated in the incoming subsections.

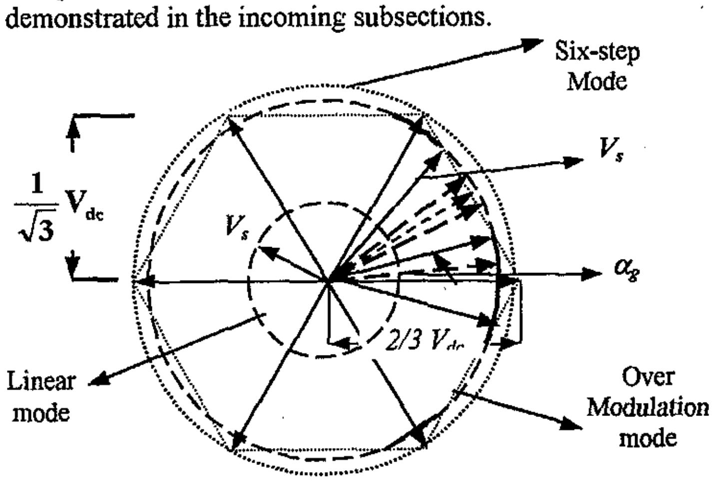

Fig. (8) SVM current controlled inverter operation modes.

6.1 *Linear mode*

To insure a sinusoidal inverter output voltage waveform, the magnitude of stator space voltage vector $V_s(t)$ must lie within the circle with radius $(1/\sqrt{3})V_{dc}$. In this case the inverter mode of operation is called linear

6.2 *Inverter operation in overmodulation range*

In SVM technique, inverter voltage vector $V_s(t)$ sometimes exceeds the value $(1/\sqrt{3})V_{dc}$ and it is still less than $(2/3)V_{dc}$, in this case the **over modulation** range is reached [6,9]. Reaching this mode of operation, the inverter loses its linear characteristics and a voltage compensation technique is required. The proposed scheme in overmodulation range will be described with reference to Fig. (8). As voltage vector increases above $(1/\sqrt{3})V_{dc}$ and still less than $(2/3)V_{dc}$, then the reference voltage vector exceeds inverter capability and therefore a modified voltage trajectory has to be set [6].

As illustrated in Fig. (8). Reaching overmodulation range, every inverter sector is divided into three regions. First region is the middle region. It is completely out of inverter capability. The other two regions are the lower and upper sides. They are within inverter capability. These three regions are defined according to the inclination angle. Therefore there are two values of α because the overmodulation circle intersects with hexagon boundaries in two points. The compensation scheme that will be applied is based on changing the inclination angle to the inverter capability regions with keeping the voltage vector amplitude constant.

$$\alpha_g = \cos^{-1}((1/\sqrt{3})V_{dc}/V_s) \tag{20}$$

Where α_g is called compensation angle.

$$\begin{aligned} \alpha_{lower} &= \frac{\pi}{6} - \alpha_g \\ \alpha_{upper} &= \frac{\pi}{6} + \alpha_g \end{aligned} \tag{21}$$

Where α_{lower} and α_{upper} are the boundaries of inverter capabilities.
Inclination angle (α) is modified according to the following conditions: -

$$\alpha = \begin{cases} \alpha & 0 \le \alpha \le \alpha_{lower} \\ (\frac{\pi}{3} - \alpha_g) & \alpha_{lower} \le \alpha \le (\frac{\pi}{6}) \\ (\frac{\pi}{3} + \alpha_g) & (\frac{\pi}{6}) \le \alpha \le \alpha_{upper} \\ \alpha & \alpha_{upper} \le \alpha \le (\frac{\pi}{6}) \end{cases} \tag{22}$$

6.3 *Inverter operation in six-step mode*

Under completely saturated conditions $V_s \geq (2/3)\, V_{dc}$, the active modulation time is kept constant at T_s and the inverter switches from circular space vector trajectory to hexagonal trajectory. This mode of operation is illustrated in Fig. (8).

7- Simulation results

The idea of event driven indicative flag is presented to demonstrate inverter operation mode. This flag takes three values, **zero** indicates linear mode, **one** indicates overmodulation mode and **two** indicates six-step mode. At rated values of motor speed, load torque and dc link voltage, the performance of **SVM** current controller operating at different switching frequencies is investigated. Figure (9) shows the performance at low switching frequency that equals **5 kHz**. The deterioration of the stator current waveform is obvious in Fig. (9-a). Figure (9-d) indicates that inverter operates most of the time at overmodulation and six-step modes. Figure (9-b) shows that the motor stator phase voltage waveform is highly distorted. When increasing the switching frequency to **10 kHz** the performance of the **SVM** current controller is better than that at **5 kHz**, as shown in Fig. (10). Figure (10-d) indicates that the inverter operation at overmodulation and six-step modes are less than that shown in Fig. (9-d). Figure (11) indicates the performance at switching frequency equals **15 kHz**. This figure shows that this performance is the best because the inverter operates all the time at the linear mode, as shown in Fig. (11-d).

In Fig. (12) statistical relationship is illustrated between f_s and the ratio of inverter operation modes. To avoid operation in relatively high ratio of six-step mode, there is a critical switching frequency (f_r) that inverter must not operate below. This frequency (f_r) is defined as the minimum frequency that inverter begins to operate totally at linear mode with no operation in six-step mode. Figure (12) indicates that this frequency is almost equal to **15.0 kHz** at rated values of motor speed, load torque and dc link voltage.

Effects of the per unit values of dc link voltage (V_{dc}) on the **SVM** are illustrated in Fig. (13) and Fig. (14). This relationship has been derived at rated motor speed and motor load. Figure (13) *demonstrates* the effects of V_{dc} on the **SVM** performance at critical switching frequency (f_r = **15.0 kHz**.). It is observed that at rated V_{dc} the ratio of inverter operation at linear mode is 100%. While reducing V_{dc}, the inverter operates most of the time at six-step mode. Figure (14) demonstrates the effects of V_{dc} on the critical switching frequency (f_r). It is observed that reducing V_{dc}, the critical switching frequency (f_r) must be increased to fulfill the required inverter operation at linear mode and then avoid distortion in stator current waveform.

The effect of motor speed on the inverter critical switching frequency (f_r), at rated values of both load and dc link (V_{dc}) is illustrated in Fig. (15). It indicates that the reference speed variations has no effect on f_r. The critical switching frequency (f_r) is constant at **15.0 kHz** regardless any motor speed variations.

The effect of motor mechanical load on the inverter critical switching frequency (f_r), at rated values of speed and dc link (V_{dc}) has been demonstrated in Fig. (16). It is obvious, from this figure, that at loads less than the rated motor load, changing motor load has no effect on the value of f_r, Also this figure shows that when overloading the inverter, f_r must be increased.

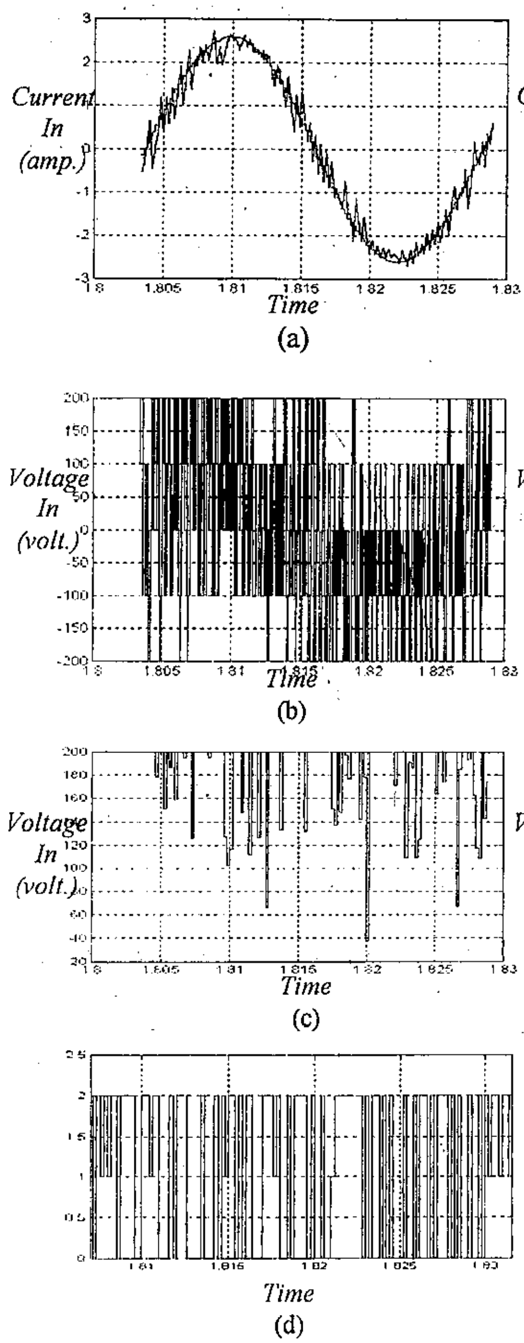

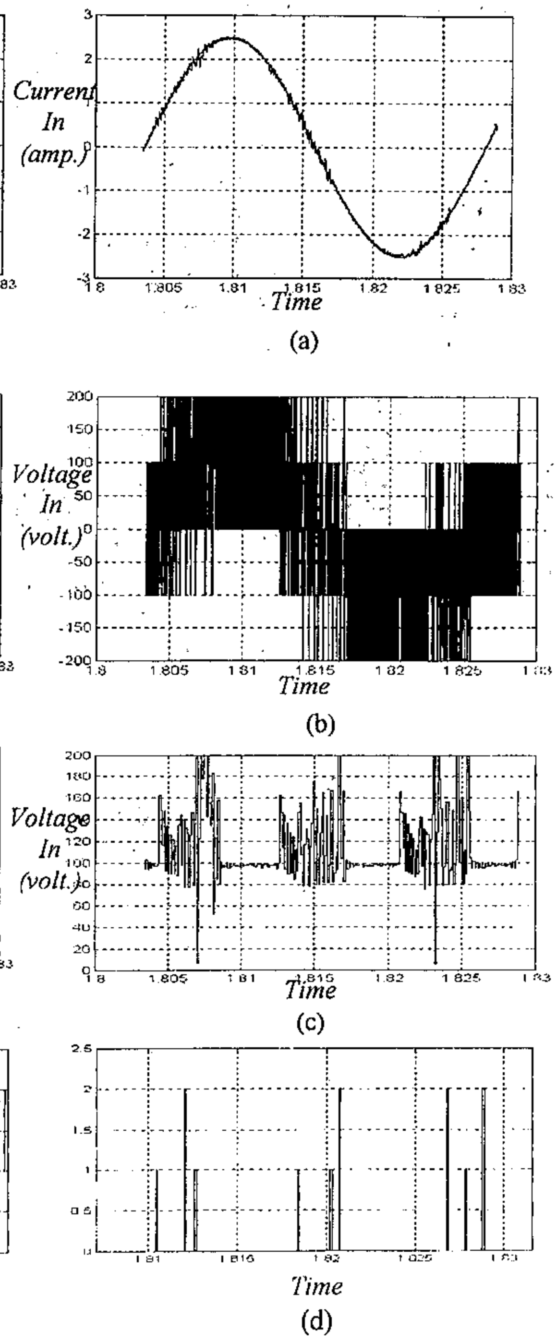

Fig. (9) **SVM** with switching frequency $\mathbf{f}_s$ =5.0 kHz.

(a) Phase (a) current waveform.
(b) Phase (a) voltage waveform.
(c) Stator voltage vector V_s waveform.
(d) Indicative flag waveform.

Fig. (10) **SVM** with switching frequency $\mathbf{f}_s$ =10.0 kHz.

(a) Phase (a) current waveform.
(b) Phase (a) voltage waveform.
(c) Stator voltage vector V_s waveform.
(d) Indicative flag waveform.

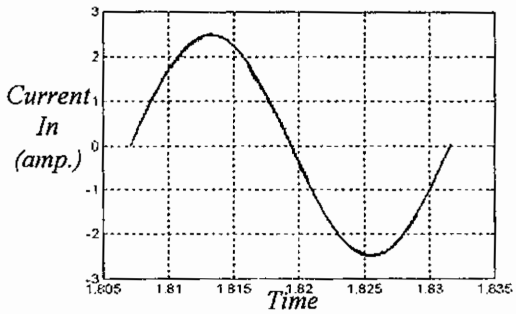

(a)

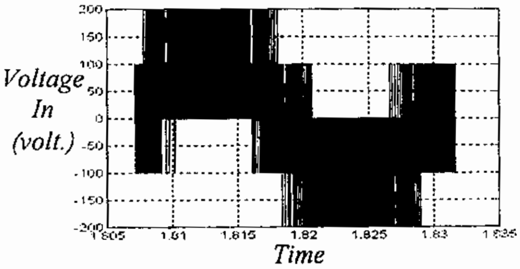

(b)

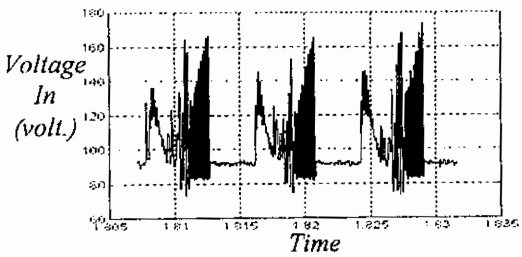

(c)

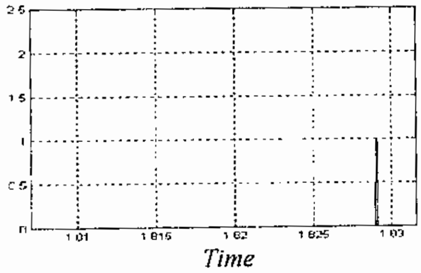

(d)

Fig. (11) **SVM** with switching frequency $\mathbf{f_s}$ =15 kHz.

(a) Phase (a) current waveform.
(b) Phase (a) voltage waveform.
(c) Stator voltage vector V_s waveform.
(d) Indicative flag waveform.

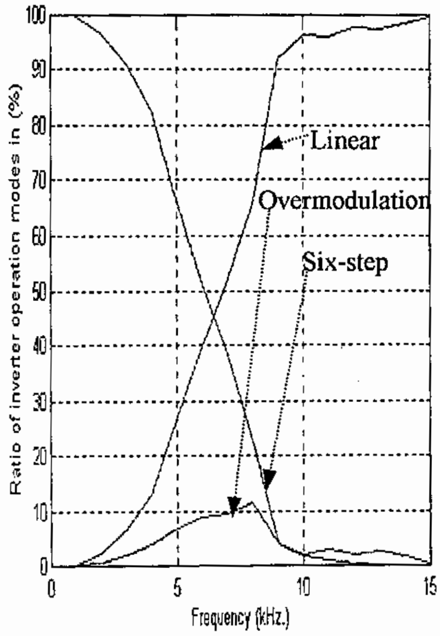

Fig. (12): Ratio of inverter operating modes at different switching frequencies.

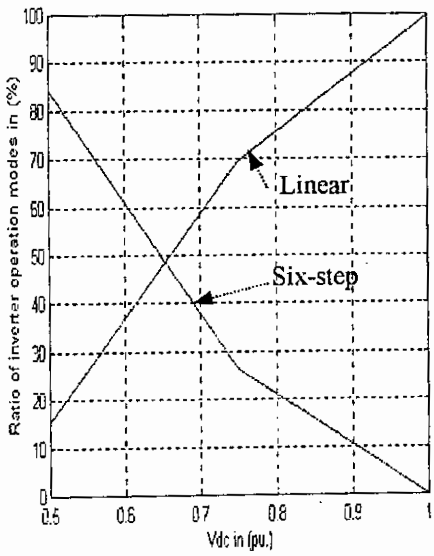

Fig. (13): Inverter operation modes at different Vdc with $\mathbf{f_s}$=15 kHz.

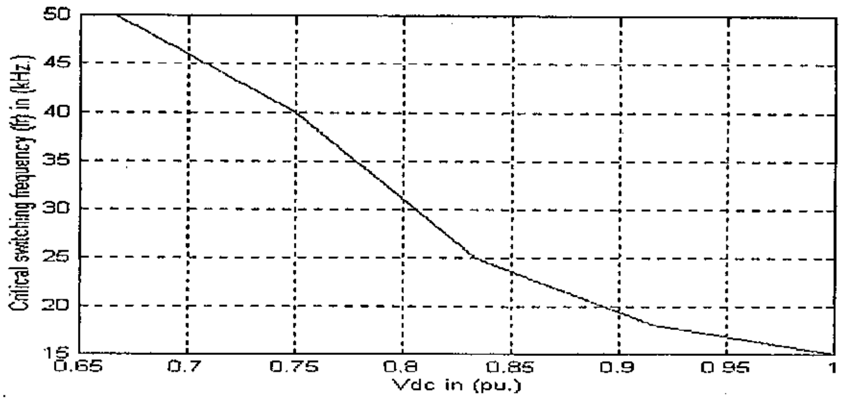

Fig. (14): The effect of Vdc on critical switching frequency (f_r).

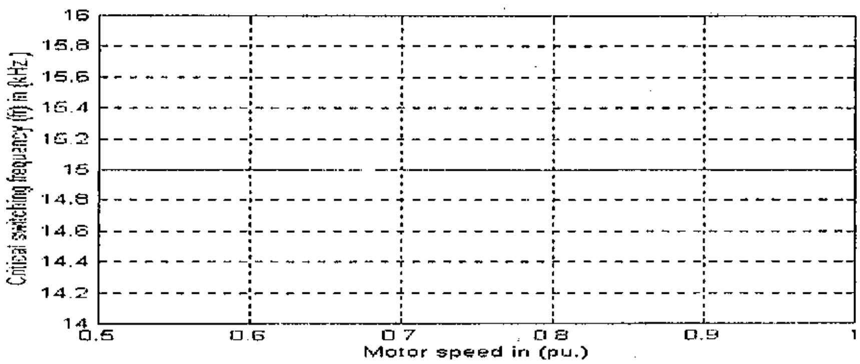

Fig. (15): The effect of motor speed on critical switching frequency (f_r).

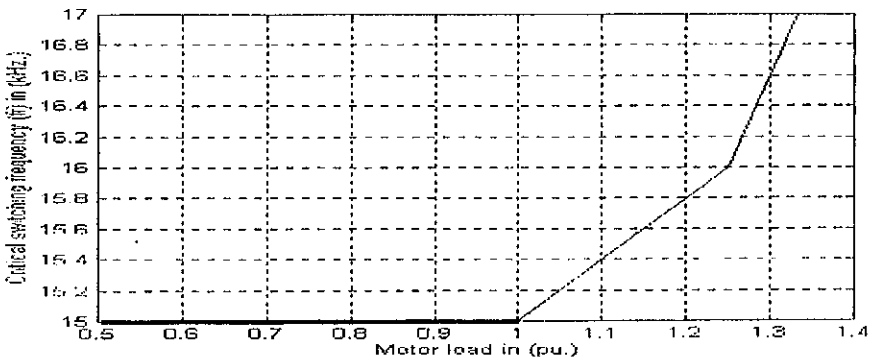

Fig. (16): The effect of motor load on critical switching frequency (f_r).

8- Conclusions

Complete inverter mathematical model and the basic concepts of **SVM** technique have been demonstrated in this paper. Inverter operation modes have been verified according to the amplitude and position of voltage vector (**$V_s(t)$**) with respect to the inverter hexagon.

It has been proved that with increasing the switching frequency, The inverter tends to operate in its linear mode. On decreasing the switching frequency, the inverter tends to operate in six-step mode, where the inverter is not capable of fulfilling the reference voltage vector V_s *(t)*. The direct result of such operation in six-step mode is the deterioration of the current wave. Statistical relationship has been developed between switching frequency and the ratio of inverter operation modes. The effects of changing dc link voltage, motor speed and mechanical load torque on the inverter modes of operation have been investigated.

9. Appendix

Motor parameters

J_m =0.003 kg.m^2

B_m=0.0008 N.m./rad./sec.

L_d=0.04244 H.

L_q=0.0796 H.

r_s=1.93 Ω

P=2

Base speed ω_b =377 rad./sec.

Current controller parameters

Kp=0.1022.

Ki= 755.0.

10- References

[1] M. Azizur Rahman, Tawfik S. Radwan, Ali M. Oshiba and Azza E. lashin " Analysis of Current Controllers For Voltage Source Inverter" IEEE Trans. Ind. Electronics, vol. 44, no. 4, pp. 477-485, August 1997.

[2] Sidney R. Bowes " Advanced Regular-Sampled **PWM** Control Techniques for Drives and Static Power Converters" IEEE Trans. Ind. Electronics, vol. 42, no. 4, pp. 367-373, August 1995.

[3] Sidney R. Bowes and Yen-Shin Lai " The Relationship Between Space vector Modulation and Regular-Sampled **PWM**" IEEE Trans. Ind. Electronics, vol. 44, no. 5, pp. 670-679,October1997.

[4] Mraian P. Kazmiekowaski and Luigi Malesani " Current Control Techniques for Three-Phase Voltage-Source **PWM** converters " IEEE Trans. Ind. Electronics, vol. 45, no. 5, pp. 691-703,October1998.

[5] Rong-Jie Tu and Chern-Lin Chen, Department of Electrical Engineering, National Taiwan University, Taipei, Taiwan " A New Space Vector **PWM** Scheme For Current-Regulated Indirect Vector Control" IECON pp.1199-1203. 1995.

[6] Selverio Bolganini and Mauro Zigliotto " Novel Digital Continuos Control of **SVM** Inverters In The Over Modulation Range" IEEE Trans. Ind. Applications, vol. 33, no. 3, pp. 525-530, March/April 1997.

[7] S. R. Bowes. Ph.D., M. I. Mech. E., F. I. E.E., and T. Daives. Ph. D. " Microprocessor-Based Development System for **PWM** Variable-Speed Drives" IEE Proceedings, vol. 132,Pt. B,. no. 1, pp. 18-45,Januery 1985.

[8] S. R. Bowes and Y. S. Lai " Investigation Into Optimizing High Switching Frequency Regular-Sampled **PWM** Control for Drives and Static Power Converters" IEE Proc. Electr. Power Appl., Vol. 143, no. 4, pp. 281-293, July 1996.

[9] P. G. Handely and J. T. Boys " Practical Real Time **PWM** Modulators: An Assessment" IEE Proc. B., Vol. 139, no. 2, pp. 96-102, March 1992.

دراسة تأثير تردد التوصيل و الفصل على أداء العاكس ذو حاكم التيار ذو موائمة فراغية إتجاهية

د/ فهمي الخولى م/ياسر البحيري د/ مصطفى الشبينى د/ عادل شبل عبد الغفار
قسم الهندسة الكهربية-كلية الهندسة بشبين الكوم-جامعة المنوفية

حاكم التيار هو الجزء الأساسي في منظومة التسيير الكهربي ذات التحكم الأتجاهى. حيث يؤثر بشكل كبير على الأداء العام لمنظومة التحكم في المحرك بشكل كبير. الوظيفة الأساسية لحاكم التيار هو التحكم في تيار الحمل للمحرك بحيث يتبع تيار الأمر المتولد من حاكم السرعة. في هذا البحث تم تقديم نموذج رياضي خاص بالعاكس المغذى لمحرك تزامني ذو مغناطيسية دائمة , على افتراض أن صمامات العاكس مثالية (لا يوجد زمن تأخير في الغلق والفتح).

هناك العديد من حواكم التيار التقليدية. مثل حاكم التيار ذو التيار المتخلف (**Hysteresis**) وحاكم التيار ذو الموجة المثلثية(**Triangular**). و لكن من أكثر حواكم التيار الحديثة والتي أصبحت مجالا مكثفا للبحث في الفترة الأخيرة هو حاكم التيار ذو الموائمة الفراغية الأتجاهية (**SVM**) . هذا النوع من حاكمات التيار يعتمد بشكل أساسي على تقريب المتجه الفراغي الخاص بجهد العضو الثابت حسب النموذج الرياضي لمتجهات جهد العاكس (**Inverter**) . يتم بعد ذلك حساب أزمنة النبضات الخاصة بأزمنة التوصيل لكل وحدات الترانزيستور لكل وجه من الثلاثة أوجه الخاص بالعاكس حسب الجهود المقربة لمتجه الجهد.

في هذا البحث تمت دراسة تأثير تغيير تردد الفتح والغلق (f_s) على كل من موجة التيار لكل وجه من الأوجه ودراسة تأثير تغيير التردد على حالة التشغيل الخاصة بالعاكس, حيث يتم تحديدها طبقا لمقدار متجه الجهد الخاص بالعضو الثابت (V_s) . هناك ثلاث حالات تشغيل للعاكس الحالة الخطية, حالة فوق الموائمة (**Overmodulation**) والست خطوات (**Six-Step**). في العادة فأن العاكس يصل لأفضل أداء عندما يعمل معظم الوقت في الحالة الخطية ولكن لوحظ في هذا البحث أنة كلما قل التردد فأن العاكس يعمل معظم الوقت في الحالتين فوق الموائمة والست خطوات مما يؤدى إلى سوء نوعية موجة التيار كلما قل التردد . تمت عمل علاقة إحصائية بين تردد الفتح والقفل و حالة تشغيل العاكس. تمت أيضا دراسة تأثير تغيير الجهد المستمر (**Vdc**) على حالات تشغيل العاكس. تمت أيضا دراسة تأثير تغيير السرعة والحمل الميكانيكي على حالة التشغيل للعاكس وتم عمل علاقات إحصائية تعبر عن هذه العلاقات.